Journal of Materials Chemistry C

Facile, Robust, Scalable Synthesis of Pd Nanoplates with Hydroxylamine as a Reducing Agent and the Mechanistic Insights from Kinetic Analysis

Journal:	*Journal of Materials Chemistry C*
Manuscript ID	TC-ART-02-2018-000928.R1
Article Type:	Paper
Date Submitted by the Author:	25-Mar-2018

Complete List of Authors:	Xia, Younan; Georgia Institute of Technology, The Wallace H. Coulter Department of Biomedical Engineering Figueroa-Cosme, Legna ; Georgia Institute of Technology Hood, Zachary; Georgia Institute of Technology, Chemistry and Biochemistry; Oak Ridge National Laboratory, Center for Nanophase Materials Sciences Gilroy, Kyle; Georgia Institute of Technology, The Wallace H. Coulter Department of Biomedical Engineering

Revised MS #TC-ART-02-2018-000928

Facile, Robust, Scalable Synthesis of Pd Nanoplates with Hydroxylamine as a Reducing Agent and the Mechanistic Insights from Kinetic Analysis

*Legna Figueroa-Cosme,[a] Zachary D. Hood,[a,b] Kyle D. Gilroy,[c] and Younan Xia[a,c]**

[a] School of Chemistry and Biochemistry, Georgia Institute of Technology, Atlanta, Georgia 30332, United States

[b] Center for Nanophase Materials Sciences, Oak Ridge National Laboratory, Oak Ridge, Tennessee 37831, United States

[c] The Wallace H. Coulter Department of Biomedical Engineering, Georgia Institute of Technology and Emory University, Atlanta, Georgia 30332, United States

[*]Corresponding author. E-mail: younan.xia@bme.gatech.edu

Abstract. Nanocrystals lined with stacking faults have received much attention in recent years due to their typical anisotropic, plate-like geometry and their perplexing formation mechanism. In this report, we introduce a simple and reliable method for the scalable production of Pd nanoplates containing stacking faults. The success of our protocol was reliant on the use of hydroxylamine as a reducing agent, which allowed for the nucleation and growth of well-defined Pd nanoplates with an average edge length of 24.5 ± 6.6 nm and thickness of 4.7 ± 0.4 nm. We conducted a kinetic analysis to validate the importance of an appropriate initial reduction rate in determining the formation of seeds lined with stacking faults. To demonstrate the robustness of this synthesis, we conducted a set of control experiments under different experimental conditions such as acidity, temperature, and chemical environment and demonstrated that Pd nanoplates could be obtained as the final products in all scenarios. We further extended the batch-based synthesis to a continuous flow reactor, moving one step closer toward high-volume production. Taken together, this method offers both simplicity and reproducibility for the synthesis of Pd nanoplates, which will enable future mechanistic studies and applications.

KEYWORDS. *Palladium, nanoplates, hydroxylamine, reducing agent, kinetic control*

Introduction

Noble-metal nanocrystals are finding use in a myriad of applications ranging from optical sensing[1] to plasmonic waveguiding,[2] biomedical research,[3] photovoltaics,[4] and heterogeneous catalysis.[5] Similar to other metals, the physicochemical properties of a Pd nanocrystal are strongly correlated with its size, shape, and internal defect structure.[6] For example, in the context of heterogeneous catalysis, the surface-to-volume ratio increases rapidly, as does the utilization efficiency of surface atoms when the size of Pd nanocrystals is reduced.[6] As for plasmonics, Pd nanocrystals with a spherical shape only exhibit localized surface plasmon resonance (LSPR) in the UV region.[7] To make Pd nanocrystals useful for photocatalytic applications that rely on sunlight for excitation, the morphology can be modified to generate highly anisotropic nanorods or nanoplates and thereby obtain LSPR peaks in the visible and near infrared (NIR) regions. To this end, it was shown that Pd nanoplates exhibit LSPR peaks in the visible region[7,8] while Zheng *et al.* reported the synthesis of Pd hexagonal nanosheets displaying strong LSPR in the NIR region.[9] As evident from these and other examples, the availability of synthetic methods capable of engineering the shape of Pd nanocrystals will be beneficial to the expansion of their properties and thus enhancement of their performance toward various applications.

During the last few decades, several groups have worked diligently to elucidate the underlying mechanisms that control the shape evolution of noble-metal nanocrystals.[10–13] When synthesized in a wet-chemical setting through homogeneous nucleation, it is generally accepted that the final shapes taken by the nanocrystals have strong correlations with the seeds formed in the very early stage, in which metal atoms agglomerate together to form fluctuating nuclei and then well-defined structures known as seeds.[14] The seeds typically exhibit one or more of the following types of internal structures, including single-crystal, singly twinned, multiply twinned, and stacking-fault-lined.[10] Recent studies have shown that both kinetics of the reaction (*e.g.*, initial

reduction rate of the metal precursor)[11,12] and structural thermodynamics (*e.g.*, relative stability of the surface and volume between the various nanostructures)[15,16] play important roles in determining the types of seeds formed during the initial stage of a synthesis. For example, one can control the production of Pd nanocrystals with shapes ranging from cuboctahedron (single-crystal) to icosahedron (multiply twinned) and nanoplate (stacking-fault-lined) by tuning the initial reduction rate of a Pd(II) precursor from relatively fast to moderate and slow, respectively.[11,12] This example illustrates how sensitive the nucleation process is to the reduction kinetics and also points to the origin of irreproducibility that troubles many nanocrystal syntheses.

Among the nanocrystals with various shapes, nanoplates are favorable in a slow reduction process and have only been obtained under kinetic control. Such highly anisotropic nanostructures are intrinsically higher in energy than other thermodynamically favored shapes such as polyhedra. Factors such as the rate of precursor reduction, atom deposition, and surface diffusion can all force the nanocrystal to evolve into a non-equilibrium shape such as the nanoplate.[10,14] Accordingly, several groups have synthesized Pd nanoplates using methods based on both polyol and aqueous systems. For example, our group synthesized Pd triangular nanoplates by controlling the reduction rate using tetraethylene glycol (TTEG) as a relatively weak reducing agent.[12] Additionally, there are reports of aqueous methods that involve the use of surfactants and reducing agents such as PVP,[7] relatively long reaction times,[7,8] and/or hazardous gases such as carbon monoxide.[9,17] All these methods have a limited window of reduction kinetics and require a fine control over experimental parameters to obtain the nanoplates. For example, if the reaction rate was slightly faster, or the concentration of reagent was not optimal, the purity and quality of the Pd nanoplates would be negatively impacted. In addition, the nature of these methods (presence of gases, polyol, long reaction times) imposes a limitation on their potential scalability and reproducibility.

In this work, we report a simple and robust method for the synthesis of Pd nanoplates using hydroxylamine as the reducing agent. Hydroxylamine is an oxygenated derivative of ammonia widely used as a reducing agent in organic syntheses but relatively unexploited in the synthesis of colloidal metal nanocrystals. Due to its good chemical stability, easy preparation, and mild reducing power, here we extend the use of hydroxylamine to the synthesis of Pd nanoplates, and also examine the effects of experimental parameters on the final product. A kinetic analysis is also conducted to shed light on the mechanistic understanding.

Experimental Section

Chemicals. Sodium tetrachloropalladate(II) (Na_2PdCl_4, 99.99%, Acros Organics), hydroxylamine hydrochloride ($NH_2OH{\cdot}HCl$, 99% Sigma-Aldrich), poly(vinyl pyrrolidone) (PVP, MW≈55,000, Sigma-Aldrich), and citric acid (CA, 99.5%, Sigma-Aldrich). De-ionized (DI) water with a resistivity of 18.2 MΩ·cm at room temperature was used throughout the experiments.

Synthesis of Pd Nanoplates in a Batch Reactor. In a standard protocol, an aqueous solution containing 100 mg PVP, 50 μL of $NH_2OH{\cdot}HCl$ (30 mM), and 1.0 mL of CA (100 mM) was prepared to a total volume of 8.0 mL. Subsequently, 1.0 mL of an aqueous solution of Na_2PdCl_4 (12 mM) was added in one shot at room temperature under magnetic stirring. The reaction was placed in an oil bath at 100 ºC and allowed to proceed for 3 h. The final product was collected by centrifugation using the Eppendorf Centrifuge 5430 at 17,000 rpm for 20 min, and then re-dispersed in water. The final product was washed three times by repeating the centrifugation protocol.

Synthesis of Pd Nanoplates in Continuous Flow. Similar to the standard protocol, an aqueous solution containing 100 mg PVP, 50 µL of $NH_2OH{\cdot}HCl$ (30 mM), and 1.0 mL of CA (100 mM) was prepared to a total volume of 8.0 mL. Subsequently, 1.0 mL of an aqueous solution of Na_2PdCl_4 (12 mM) was added in one shot at room temperature under magnetic stirring. The prepared reaction solution was injected using a syringe pump (2 mL min^{-1}) to a PVC tubing system preheated at 80 ºC (see references [24] and [25] for a visual description of the system, and the dimensions of the tubing). Once the reaction solution was completely injected in the tubing, it was allowed to proceed for 3 h. The final product was collected by injecting air to the PVC tubing and place in centrifugation vials for washing. We used the Eppendorf Centrifuge 5430 operated at 17,000 rpm for 20 min. The product was then re-dispersed in water and washed three times following the same parameters.

Kinetic Studies. The reduction kinetics were determined by measuring the concentration of Pd(II) ions remaining in the reaction solution at different time points of a synthesis. Two methods were used to determine the kinetics: *i*) analyzing a number of identically prepared vials, and *ii*) analyzing aliquots sampled from a single vial. In the first method, a number of identically prepared reaction vials were placed simultaneously in the same oil bath. Then, one reaction vial was removed from the oil bath at a specific time point (*e.g.*, 15, 30, 60 min) and the reaction was quenched by placing the vial in an ice bath. Aliquots of 0.2 mL were taken from the quenched reaction solution and injected into 0.8 mL of aqueous KBr (500 mg/mL). In the second method, aliquots of 0.2 mL were taken from a single vial (note: the vial was frequently uncapped in this case) and injected into 0.8 mL of cold KBr solution (500 mg/mL) to quench the reaction. Because of the high concentration of bromide ions, the unreacted Pd(II) ions quickly undergo ligand exchange to generate the

complex of $PdBr_4^{2-}$ for UV-vis analysis.[12] The aliquot obtained from both methods were centrifuged at 55,000 rpm for 30 min to remove all the Pd nanoparticles, and the supernatants were used to measure the concentrations of $PdBr_4^{2-}$ ions by UV–vis spectroscopy. The measured absorbance at 332 nm and a calibration curve (see reference [12] for the procedure) were used to determine the concentrations of the remaining Pd(II) ions at different reaction times. Each data point represents two repeated measurements.

Characterization. Samples were characterized using a transmission electron microscope (Hitachi HT7700) operated at 120 kV. High-resolution transmission electron microscopy (HRTEM) was performed on an aberration-corrected FEI Titan S 80-300 STEM/TEM microscope equipped with a Gatan OneView camera at an acceleration voltage of 300 kV. All samples for HRTEM were prepared by drop casting 8 μL of the as-prepared aqueous dispersions of Pd nanoplates on lacey carbon-coated copper grids. The X-ray diffraction (XRD) analysis was performed using the Empyrean PANalytical system with an K-Alpha1 radiation source of wavelength 1.54 Å, operated at 45 kV. The sample was prepared by drop casting the washed aqueous suspension of Pd nanoplates onto a silica wafer and then dried at room temperature overnight. The data was analyzed using Origin software, a background subtraction was performed to present the XRD data in this report. The analysis of the reduction kinetics was performed using an UV-vis spectrophotometer (Cary 60, Agilent Technology) in the spectral region of 200−800 nm. The pH measurements were performed using a Fisher Scientific Accumet Basic AB15 pH meter.

Results and Discussion

For the synthesis of Pd nanoplates, we used Na_2PdCl_4 as a salt precursor, hydroxylamine as the primary reducing agent, PVP as a surfactant, and CA as a capping agent toward Pd(111) surface. In a standard protocol, an aqueous solution containing PVP, hydroxylamine, and CA was prepared at room temperature. Subsequently, an aqueous solution of Na_2PdCl_4 was added in one-shot under magnetic stirring, followed by heating at 100 ºC in an oil bath.

Figure 1A shows the TEM image of a typical sample of Pd nanoplates, which had an average edge length of 24.5 ± 6.6 nm and thickness of 4.7 ± 0.4 nm. In this sample, we have both hexagonal (~70%) and triangular (~30 %) nanoplates. We used HRTEM to analyze the atomic structure of the Pd nanoplates. The individual hexagonal plate shown in Figure 1B was oriented along its [111]-zone axis, as evident by the hexagonal geometry and packing of atoms as highlighted in the inset. To determine the thickness and further analyze the crystal structure of the Pd nanoplates, we drop-casted their suspension on a copper TEM grid coated with lacey carbon. We were able to locate individual nanoplates oriented with the edges and {111} facets perpendicular and parallel to the electron beam, respectively. This allowed us to perform HRTEM imaging of atomic columns along the lateral direction of an individual nanoplate (see Figure 1C and the red-dashed lines that partially highlight the stacking fault line). An enlarged view of the HRTEM can be found in Figure S1 of the supporting information. From the HRTEM image, we were able to obtain a *d*-spacing of around 2.25 Å for the (111) planes, a value consistent with the JCPDS datum of 2.24 Å. We also performed an XRD analysis of the Pd nanoplates. Most notably, the (111) peak at $2\theta = 40.2°$ is predominantly stronger than the (200) peak at $2\theta = 46.7°$ and the (220) peak at $2\theta = 68.3°$ (even considering the structure factors), suggesting that most of the nanoplates were oriented such that their large flat {111} faces were parallel to the surface of the sample stage. This result also suggests that our

sample was high in purity. From the XRD pattern we obtained a value of 2.24 Å for d_{111}, which is consistent with the aforementioned JCPDS value.

The exact mechanism of nanoplate formation is still unknown and the underlying question is in the nucleation process involved in the formation of the seed. It has been suggested that the key factor for the formation of nanoplates is a relatively slow reduction rate for the generation of stacking faults during seed formation.[18] To test this hypothesis, we monitored the progress of the reaction using UV-vis spectroscopy and then compared the spectra to the product formed at different points during the synthesis. We set up a number of parallel reactions in the same oil bath and simultaneously started the timer (Note: all vials were firmly capped). One reaction vial was taken out from the oil bath at a specific time point and immediately placed in an ice bath to quench the reduction. After removing the solid products by centrifugation, we analyzed the concentration of Pd(II) in the supernatant using UV-vis spectroscopy. As shown in Figure 2A, the intensity of the absorption peak associated with Pd(II) decreased with time, which can be attributed to the reduction by hydroxylamine for the generation of Pd nanoplates. By fitting the linear plot in Figure 2B and using a conversion factor from minute to second, we obtained a rate constant of $k = 3.0 \times 10^{-4}\ s^{-1}$ for the reduction reaction. When combined with the initial concentration of $PdCl_4^{2-}$ in the reaction solution (1.2 mM by taking into account the dilution factor), we obtained an initial reduction rate of $R_0 = 3.6 \times 10^{-7} M \cdot s^{-1}$. This value falls into the range responsible for the formation of stacking faults, in agreement with our previous report.[12]

To analyze the evolution of the nanoplates, we imaged the nanocrystals formed at 15, 30, 60, and 180 min of a synthesis using TEM. The formation of plate-like structures was evident even at the very beginning of a synthesis (Figure 3A), and their average edge length then increased from 4 to 10, 14, and 25 nm (Figure 3, B-D). Also, the size distribution narrowed with reaction time,

suggesting that Ostwald ripening played a role in the formation of the relatively large nanoplates. It is worth mentioning that the growth of nanoplates appeared to be preferentially along the lateral directions since the edge length increased from 4.2 nm to 25–30 nm, in contrast to the thickness that remained around 4.7 nm. This trend is also consistent with the proposed mechanism for the formation of Ag nanoplates.[18]

Interestingly, when the reaction was performed in a single vial and aliquots were taken at different time points (note: the vial was constantly uncapped in this case), the reaction kinetics was different and thus the products were also different. As shown in Figure 4A and B, the kinetics show a two-step reduction process where the initial reduction occurred very slowly and then suddenly accelerated after 60 min, which could be attributed to the accelerated reduction of metal precursor by auto-catalytic reduction.[12,19] As shown in Figure 4C-F, the Pd nanoplates exhibited a rounded profile, which promotes us to ask whether oxidative etching was occurring during the kinetic studies because of the constant exposure to air when extracting aliquots.

We performed additional syntheses to explore the role of the dissolved gases on the final products. Four reaction vials were prepared including: *i*) an uncapped vial and thus constantly exposed to air, *ii*) a capped vial and thus not exposed to air, *iii*) a capped vial purged with pure nitrogen, and *iv*) a capped vial purged with pure oxygen. Note that the syntheses involving nitrogen and oxygen, experiments (iii) and (iv), were purged with the respective gases for 30 min. As shown in Figure 5, the morphology of the products under air, oxygen, and nitrogen environment did not differ significantly, which suggests that oxidative etching can be excluded as a cause for the rounding of the nanoplates. A plausible explanation for this observation should thus be attributed to N_2O, the oxidation product of hydroxylamine. The formation of N_2O gas was observed by Bengtsson-Kloo *et al.* when studying the oxidation of hydroxylamine by iron(III).[20-22] We posit

that the process of opening the vial for the kinetic measurements may have relieved some of the pressure, allowing the N_2O to escape from the reaction solution, which could have a certain role in controlling the shape of the Pd nanoplates. However, we have to point out that the extent of N_2O production and the exact role of N_2O are yet to be completely determined.

The reducing power of hydroxylamine strongly depends on pH,[21] and therefore, even slight changes to the pH are expected to impact the kinetics and correspondingly the shape and structure of the Pd products.[12] For this reason, we determined if the presence of CA would affect the outcome of a synthesis by performing a series of control experiments. When only using hydroxylamine in the reaction solution (*i.e.*, in the absence of CA), the solution pH was 3.8 rather than 2.7, and we observed two populations of particles: Pd nanoplates with an average edge length of 15 ± 4 nm and relatively large (around 75 nm) particles with unidentifiable internal defect structures, see Figure S2A. These results suggest that the change to pH could play a critical role in controlling the final product. It should be noted that CA could also serve as a capping agent since computational calculations have suggested that CA had a strong propensity to bind to Pd(111).[23] To corroborate if the acidic environment was, in fact, assisting the formation of plates, we changed CA to ascorbic acid, a compound commonly used solely as a reducing agent. As shown in Figure S2B, we obtained Pd nanoplates with an average edge length of 18 ± 1 nm. These results suggest that the acidic environment could slow down the reaction kinetics to favorably support the formation of nanoplates. Also, the slightly bigger size of the nanoplates also suggest a slower reduction, because less seeds would be formed at the beginning of reaction and thus bigger particles. However, similar to CA, ascorbic acid might be interacting with the surface of the Pd nanocrystals too,[23] and it could also be serving as a reducing agent, making it very difficult to isolate the precise roles of the individual additives.

Despite the evident impact of hydroxylamine and the different acids had on the formation of Pd nanoplates, we are still uncertain about the exact reduction mechanism. The PVP introduced as a colloidal stabilizer could also act as a reducing agent itself.[24] Therefore, we conducted the reaction in the absence of hydroxylamine. As shown in Figure S2C, a mix of different Pd nanocrystals were formed with sizes around 14 ± 2 nm, but with clearly no control over the shape and internal twin structure. This result indicates that PVP does have reducing power, but it cannot be used solely as a reducing agent for the formation of Pd nanoplates in our experiments. As shown in the UV-vis spectra of Figure S3, the introduction of PVP or CA did not cause significant changes to the absorption peak position of the Pd(II) complex, suggesting their negligible role in coordinating to Pd(II) ions relative to other ligands such as chloride and water. Taken together, we believe that PVP mainly served as a co-reductant and a colloidal stabilizer during the formation of the Pd nanoplates.

Our method for the synthesis of Pd nanoplates does not require organic solvents. It is also simple and robust, making it ideal to explore its scalability for high-volume production. To date, there are no reports on the synthesis of Pd nanoplates using a continuous flow system. Here we successfully extended the synthesis to a continuous flow reactor and obtained Pd nanoplates with quality compatible to those obtained in a batch reactor. Both the syntheses in batch and continuous flow reactors were conducted at a lower temperature of 80 °C than the standard protocol. As shown in Figure 6, Pd nanoplates could be obtained at this lower temperature and in a completely different reaction batches.

Conclusion

We have demonstrated a robust synthesis of Pd nanoplates using hydroxylamine as the reducing agent. By characterizing the products obtained at different time points, we found that the internal defect structure of the Pd nanoplates was formed at the early stage of a synthesis, which provided seeds with stacking-faults for the subsequent growth into highly anisotropic, planar, well-defined hexagonal nanoplates. It is reasonable to consider this synthesis a *robust* one because we found that rather drastic changes to the experimental parameters such as pH, temperature, and chemical environment did not significantly alter the nucleation process (*e.g.*, formation of internal defect structure) and overall shape (*e.g.*, hexagonal) of the final products. In addition, our protocol could even be adapted for use in a continuous flow reactor to scale up the production of high quality Pd nanoplates. Taken together, we strongly believe that this particular system can serve as a model reaction for future experiments with an aim to elucidate the mysterious mechanisms occurring during the homogeneous nucleation of both stacking-fault-lined structures and other unique defect containing nanocrystals.

Acknowledgments

This work was supported in part by a DOE subcontract from the University of Wisconsin-Madison (DE-FG02-05ER15731). TEM imaging and XRD were performed at the Georgia Institute of Technology's Institute of Electronics and Nanotechnology (IEN) characterization facilities. HR-TEM imaging was performed at the Center for Nanophase Materials Sciences, which is a DOE Office of Science User Facility. ZDH gratefully acknowledge a Graduate Research Fellowship award from National Science Foundation (DGE-1650044) and Georgia Tech-ORNL fellowship.

Also, we would also like to thank Dr. Thenner Silva Rodrigues and Dr. Anderson G. M. da Silva for the helpful discussion regarding this work.

References

[1] C. Langhammer, Z. Yuan, I. Zoric and B. Kasemo, *Nano Lett.*, 2006, **6**, 833.

[2] J. R. Krenn, *Nature Mater.*, 2003, **2**, 210.

[3] M. B. Kimmey, X. Li and Y. Xia, *Nano Lett.*, 2005, **5**, 473.

[4] D. M. Schaadt, B. Feng and E. T. Yu, *Appl. Phys. Lett.*, 2005, **86**, 063106.

[5] E. M. Larsson, C. Langhammer, I. Zoric and B. Kasemo, *Science*, 2009, **326**, 1091.

[6] Y. Xia, Y. Xiong, B. Lim and S. E. Skrabalak, *Angew. Chem. Int. Ed.*, 2009, **48**, 60.

[7] Y. Xiong, J. M. McLellan, J. Chen, Y. Yin, Z.-Y. Li and Y. Xia, *J. Am. Chem. Soc.*, 2005, **127**, 17118.

[8] Y. Xiong, I. Washio, J. Chen, H. Cai, Z.-Y. Li and Y. Xia, *Langmuir*, 2006, **22**, 8563.

[9] X. Huang, S. Tang, X. Mu, Y. Dai, G. Chen, Z. Zhou, F. Ruan, Z. Yang and N. Zheng, *Nat. Nanotechnol.*, 2011, **6**, 28.

[10] Y. Xiong and Y. Xia, *Adv. Mater.*, 2007, **19**, 3385.

[11] T.-H. Yang, K. D. Gilroy and Y. Xia, *Chem. Sci.*, 2017, **8**, 6730.

[12] Y. Wang, H.-C. Peng, J. Liu, C. Z. Huang and Y. Xia, *Nano Lett.*, 2015, **12**, 1445.

[13] W. Niu, L. Zhang and G. Xu, *ACS Nano*, 2010, **4**, 1987.

[14] K. D. Gilroy, H.-C. Peng, X. Yang, A. Ruditskiy and Y. Xia. *Chem. Commun.*, 2017, **53**, 4530.

[15] K. D. Gilroy, A. O. Elnabawy, T.-H. Yang, L. T. Roling, J. Howe, M. Mavrikakis and Y. Xia, *Nano Lett.*, 2017, **17**, 3655.

[16] K. D. Gilroy, J. Puibasset, M. Vara and Y. Xia, *Angew. Chem.*, 2017, **129**, 8773.

[17] H. Li, G. Chen, H. Yang, X. Wang, J. Liang, P. Liu, M. Chen and N. Zheng, *Angew. Chem. Int. Ed.*, 2013, **52**, 8368.

[18] J. Zeng, J. Tao, W. Li, J. Grant, P. Wang, Y. Zhu and Y. Xia, *Chem. Asian J.*, 2011, **6**, 376.

[19] T.-H. Yang, S. Zhou, K. D. Gilroy, L. Figueroa-Cosme, Y.-H. Lee, J.-M. Wu and Y. Xia, *Proc. Natl. Acad. Sci. USA*, 2018, **114**, 13619.

[20] G. Bengtsson, S. Fronæus and L. Bengtsson-Kloo, *J. Chem. Soc., Dalton Trans.*, 2002, 2548.

[21] J. Li and X. Lin, *Sensor Actuat. B-Chem.*, 2007, **126**, 527.

[22] M. D. Johnson and B. J. Hornstein, *Inorg. Chem.*, 2003, **42**, 6923.

[23] J. Yue, Z. Du and M. Shao, *Chem. Phys. Lett.*, 2016, **659**, 159.

[24] L. Zhang, Y. Xia, *Adv. Mater.* 2014, **26**, 2600.

[25] L. Zhang, G. Nui, N. Lu, J. Wang, L. Tong, L. Wang, M. Kim, Y. Xia, *Nano Lett.* 2014, **14**, 6626.

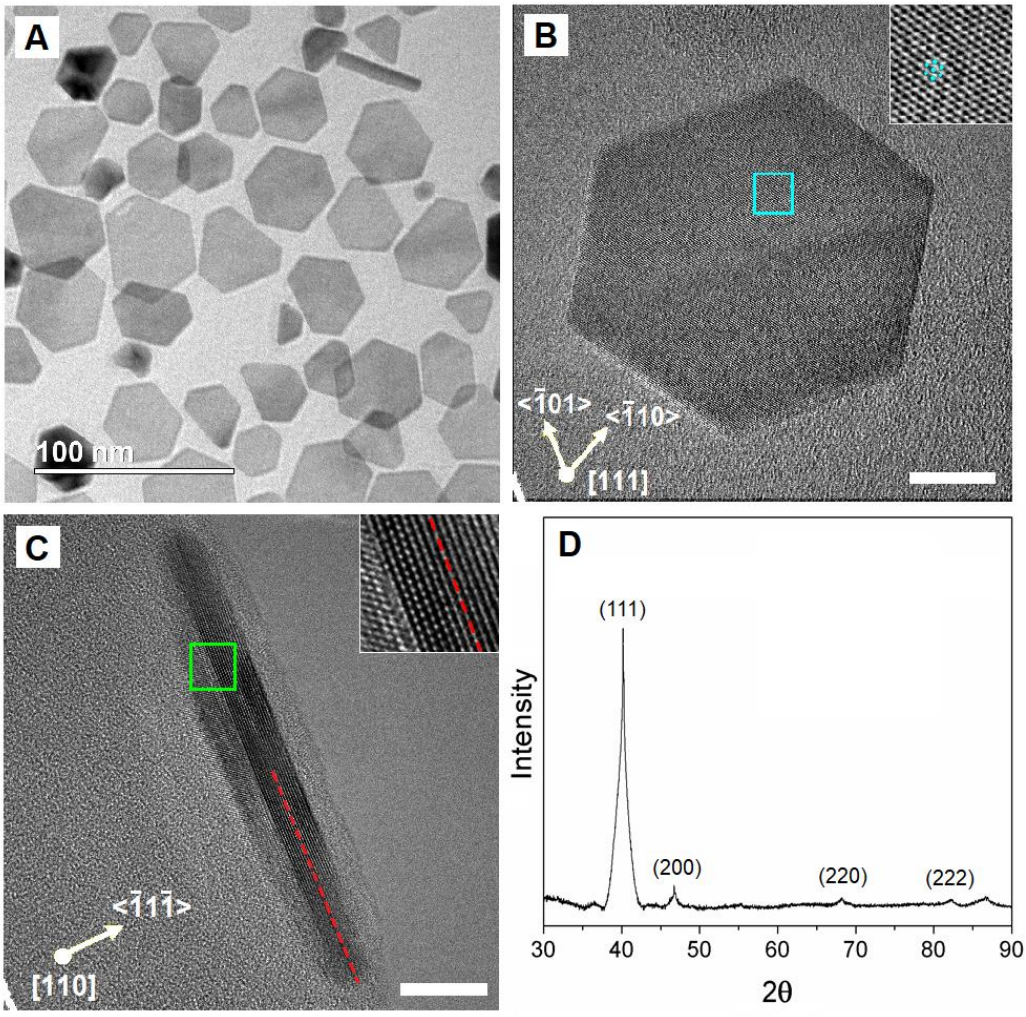

Figure 1. (A) TEM image of a typical sample of Pd nanoplates prepared using the standard protocol. (B, C) HRTEM images of an individual nanoplate imaged from (B) the top surface with an orientation along its [111]-zone axis (inset: a magnified view of the boxed region) and (C) the side surface with an orientation along its [110]-zone axis (inset: a magnified view of the atoms in the green box). The red-dashed lines partially mark the stacking-fault plane. (D) X-ray diffraction pattern of the Pd nanoplates, indicating that the nanoplates were crystallized in the *fcc* structure and they tended to lie flat, with (111) planes parallel to the substrate surface, during drop-casting. Scale bars: 10 nm.

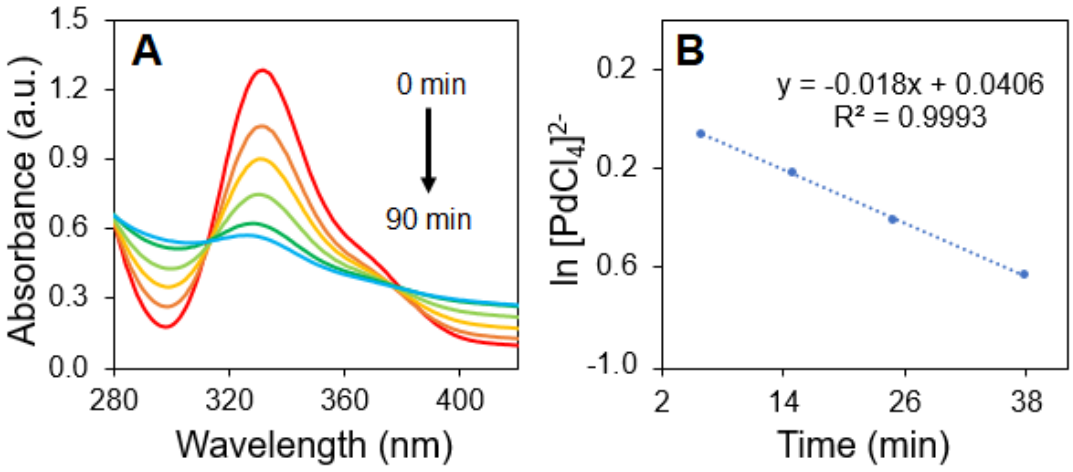

Figure 2. (A) UV-vis spectra showing the change in absorbance for the Pd(II) ions over a course of 60 min. (B) Log-plot trending the concentration of the remaining Pd(II) precursor as the reaction proceeds.

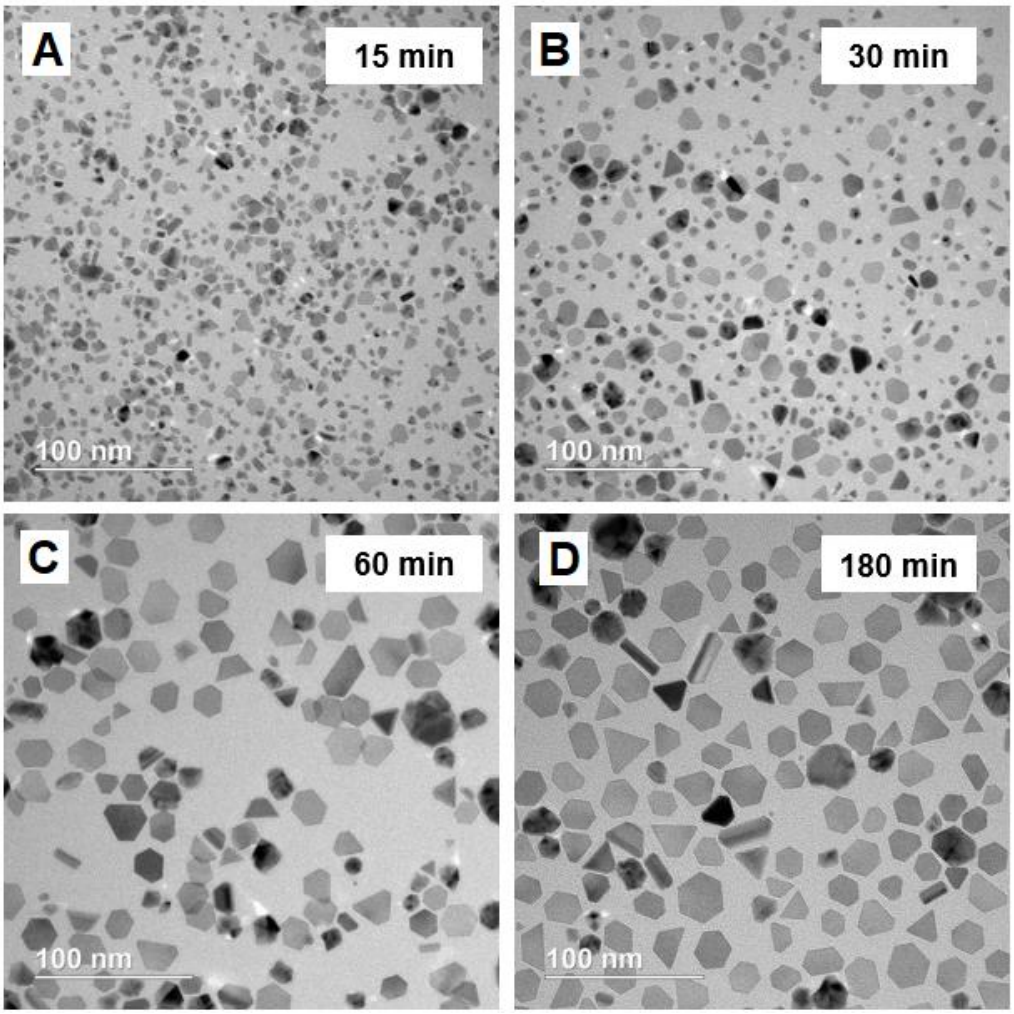

Figure 3. TEM images of the products of a standard synthesis when the reduction was quenched after reacting for (A) 15, (B) 30, (C) 60, and (D) 180 min.

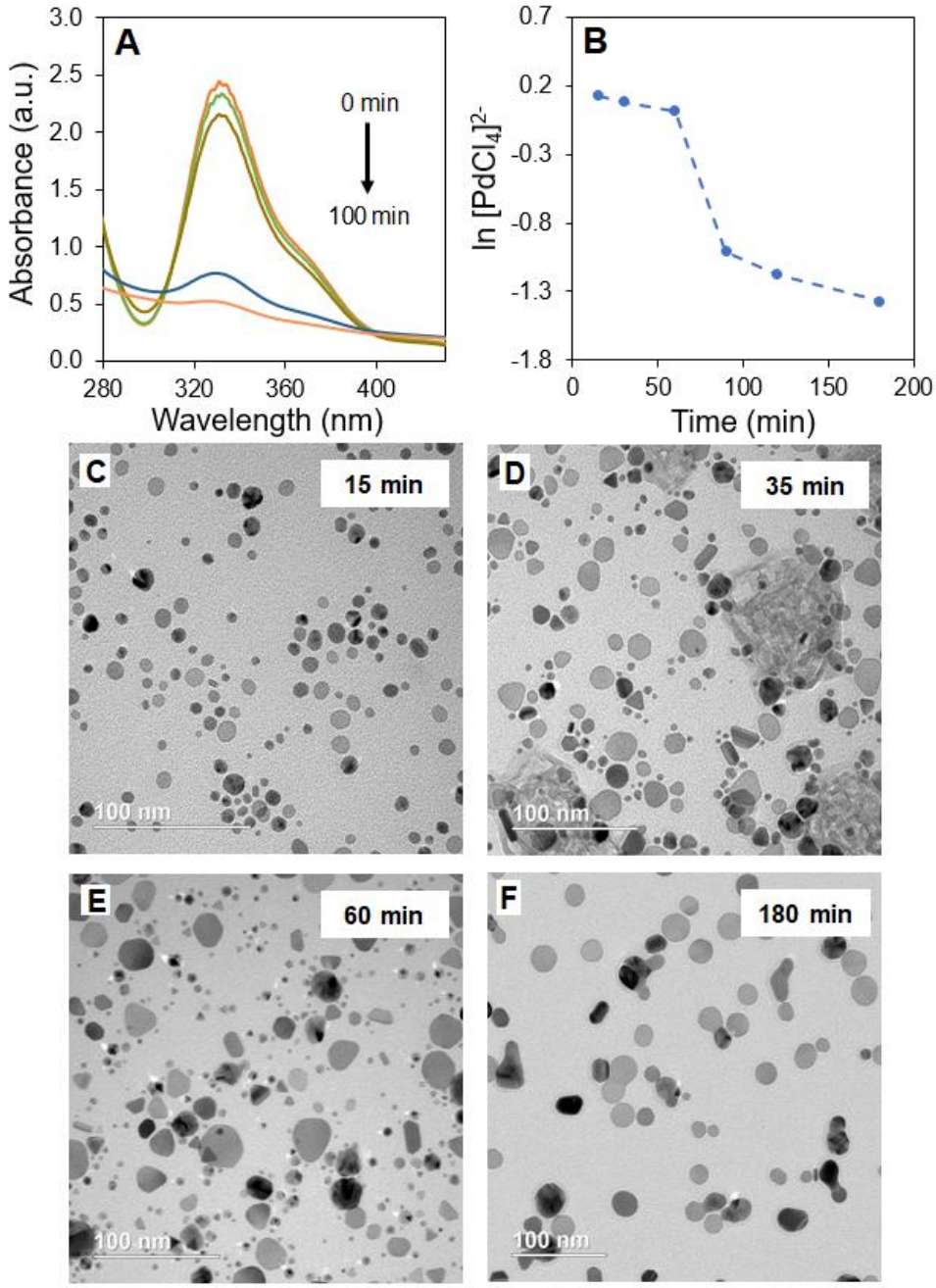

Figure 4. (A) UV-vis spectra tracking the change in absorbance for the Pd(II) precursor over a course of 120 min, during which the vial was uncapped to sample aliquots for UV-vis and TEM analyses. (B) Plot trending the concentration of the remaining Pd(II) precursor as a function of reaction time. (C-F) TEM images of the solid products obtained at (C) 15, (D) 35, (E) 60, and (F) 180 min, into the synthesis.

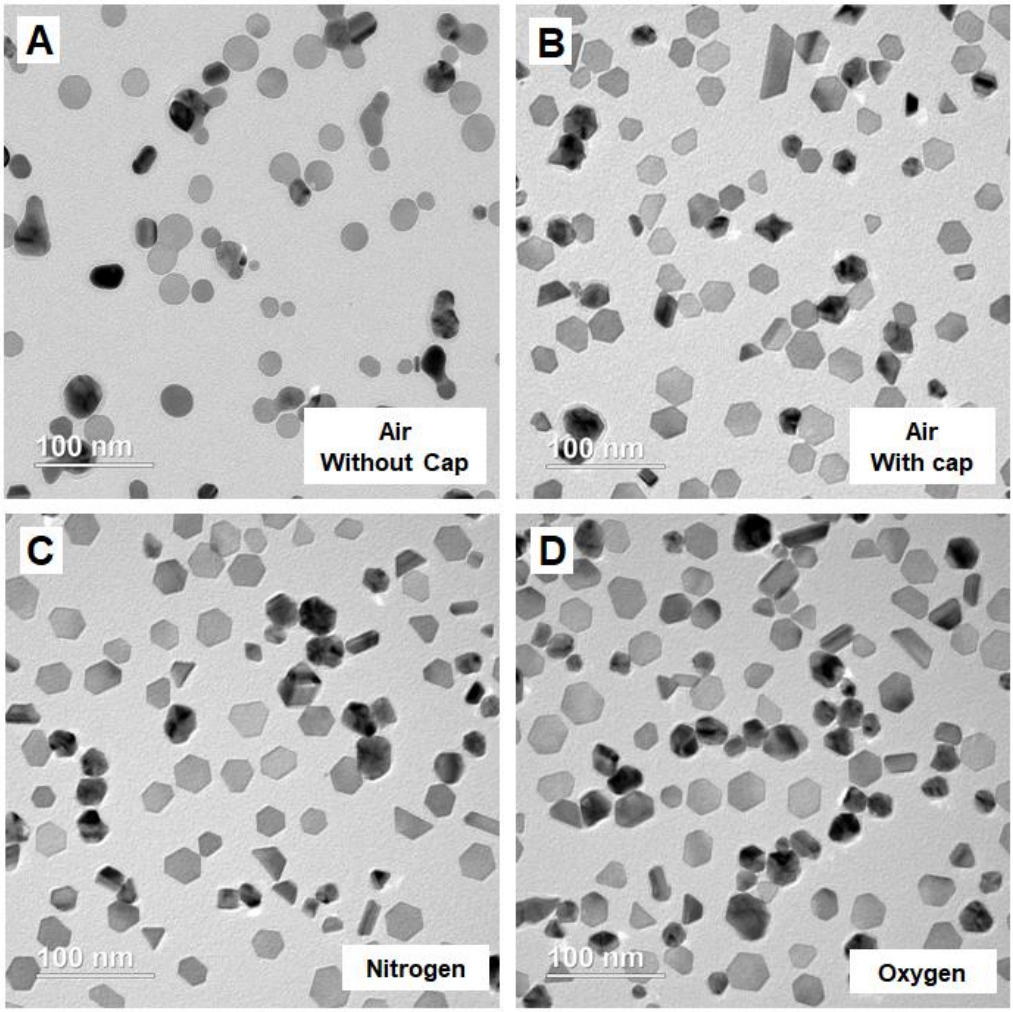

Figure 5. TEM images of Pd nanoplates formed under different reaction conditions by varying the gases in the reaction vials: (A) no capping, (B) tightly capped, (C) nitrogen purging and then tightly capping, and (D) oxygen purging and then tightly capped.

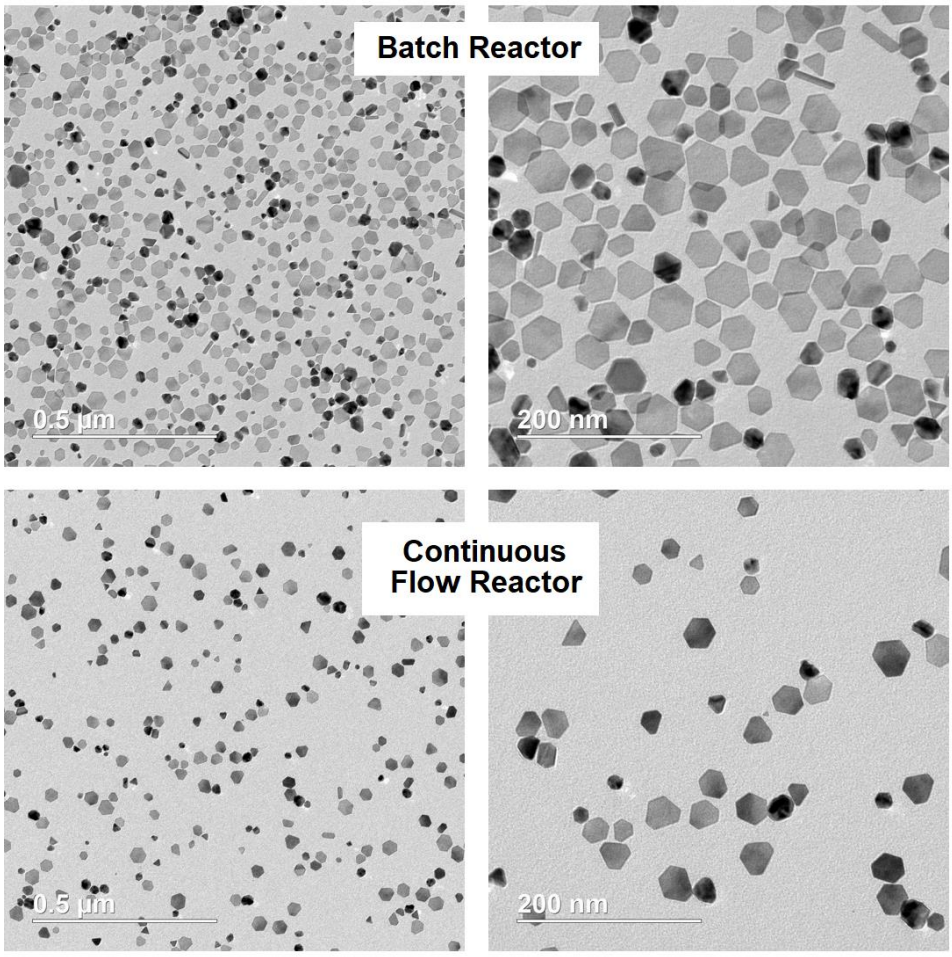

Figure 6. TEM images of Pd nanoplates obtained in a batch reactor (vial) and a continuous flow system (PTFE tube), respectively. Note that the protocol was slightly modified to accommodate the continuous flow synthesis by reducing the temperature from 100 to 80 °C.

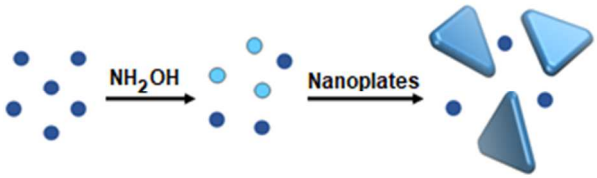

We report a simple and robust synthesis of Pd nanoplates using hydroxylamine as reductant, and the kinetic analysis.